Conformational and Structural Relaxations of Poly(ethylene oxide) and Poly(propylene oxide) Melts: Molecular Dynamics Study of Spatial Heterogeneity, Cooperativity, and Correlated Forward–Backward Motion

Michael Vogel

Institut für Physikalische Chemie, Westfälische Wilhelms-Universität Münster, Corrensstr. 28/30, 48149 Münster, Germany

Received October 30, 2007; Revised Manuscript Received February 6, 2008

ABSTRACT: Performing molecular dynamics simulations for all-atom models, we characterize the conformational and structural relaxations of poly(ethylene oxide) and poly(propylene oxide) melts. The temperature dependence of these relaxation processes deviates from an Arrhenius law for both polymers. We demonstrate that mode-coupling theory captures some aspects of the glassy slowdown, but it does not enable a complete explanation of the dynamical behavior. When the temperature is decreased, spatially heterogeneous and cooperative translational dynamics are found to become more important for the structural relaxation. Moreover, the transitions between the conformational states cease to obey Poisson statistics. In particular, we show that, at sufficiently low temperatures, correlated forward–backward motion is an important aspect of the conformational relaxation, leading to strongly nonexponential distributions for the waiting times of the dihedrals in the various conformational states.

I. Introduction

Understanding the glass transition of polymer melts is of enormous interest from the viewpoints of fundamental and applied science. When polymer melts or other glass-forming liquids are cooled, the structural relaxation slows down tremendously, and eventually, an amorphous solid, a glass, is formed at the glass transition temperature, T_g. The structural relaxation or, equivalently, the α relaxation of most glass-forming liquids exhibits two striking features: its time dependence differs from a single-exponential function, and its temperature dependence deviates from an Arrhenius law.[1]

Molecular dynamics (MD) simulations have proven a powerful tool to investigate the initial stages of the glassy slowdown of the structural relaxation in moderately viscous liquids.[2–6] Most of these studies focused on simple model-glass formers, e.g., binary Lennard-Jones mixtures. In MD simulations of glass-forming polymer melts, coarse-grained models were used, while investigations on chemically realistic models are more rare.[5,6] For the latter models, consideration of all the interactions associated with the connectivity, e.g., of the energy barriers against the conformational dynamics, interferes with the necessity to follow the slowdown of the molecular dynamics over broad temperature and time ranges due to the limited computer power. However, the rapid development of computer technology steadily improves the possibilities, and very recently, chemically realistic polymer models have started to become an important tool to study the mechanisms for the primary and Johari−Goldstein secondary relaxation processes in polymer melts.[7,8]

The mode-coupling theory (MCT), which focuses on density fluctuations, has been put forward to explain the observation that the temperature-dependent structural relaxation times deviate from an Arrhenius law for most glass-forming liquids.[9] In its idealized version, MCT predicts a power-law divergence of the α relaxation time at a critical temperature, T_c. MD simulations were employed to test the predictions of MCT for moderately viscous liquids. It was found that this theory captures many aspects of the glassy slowdown for several simple model-glass formers, including a bead−spring polymer model,[6,10,11] while the applicability to all-atom polymer models was controversially discussed.[5,8,12,13] In any event, T_c is substantially higher than T_g, indicating that MCT fails to describe the molecular dynamics in highly viscous liquids.[1] Therefore, it is important to consider further aspects of glass-forming liquids, and approaches focusing on the cooperativity and heterogeneity of the structural relaxation have received considerable attention.[14,15]

Various experimental observations demonstrated that the nonexponential α relaxation of glass-forming liquids is related to the effect that the molecular dynamics are heterogeneous; i.e., it is possible to select particles that rotate or translate much farther or shorter distances than an average particle.[16–18] However, most experimental techniques provide only limited information about the spatial distribution of particles showing different mobilities. Recent nuclear magnetic resonance approaches demonstrated for various glass-forming liquids, including a polymer melt, that the dynamics are spatially heterogeneous.[19–21] Specifically, particles within a physical region of the liquid show an enhanced or diminished mobility as compared to particles in a region a few nanometers away. Nevertheless, a detailed experimental characterization of the time and temperature dependence of spatially heterogeneous dynamics is still lacking.

MD simulations provide straightforward access to spatial correlations of the particle mobility.[3,6] Work on simple models of atomic and polymeric glass-forming liquids reported that highly mobile and highly immobile particles aggregate into clusters, which are transient in nature.[22–29] The clusters of highly mobile particles are largest in the very early stages of the α relaxation. Upon cooling, the cluster size increases and a divergence near the critical temperature T_c was proposed.[24–26] Moreover, it was demonstrated that stringlike motion is an important channel for the structural relaxation of the highly mobile particles.[29–31] This means that mobile particles tend to follow each other along one-dimensional paths. The existence of spatially heterogeneous dynamics is not restricted to simple models, but this effect was also observed for more complex models of glass-forming liquids, namely, for models of propylene carbonate, water, and silica.[32–36] Interestingly, the coopera-

10.1021/ma7024072 CCC: $40.75
Published on Web 03/25/2008

tive stringlike motion was found to be of little relevance for the silicon atoms in the silica model, where the structural relaxation follows an Arrhenius law.[34,35]

It was argued that the structural relaxation differs between bead−spring and all-atom polymer models.[5] Specifically, conformational dynamics are of central importance for the latter, but not for the former models. For all-atom polymer models, the slowdown of the α relaxation was argued to depend not only on intermolecular packing effects, as assumed in MCT, but also on intramolecular torsional barriers.[5,8,12,13] Moreover, previous work showed that the conformational relaxation is by no means a simple relaxation process, but it involves, e.g., pronounced dynamical heterogeneities.[7,37,38] In view of all these results, it becomes apparent that improving our understanding of the polymer glass transition requires a detailed characterization of the interplay of the intra- and intermolecular aspects of the molecular dynamics.

Here, we perform MD simulations for all-atom models of poly(ethylene oxide) (PEO) and poly(propylene oxide) (PPO). Because of the capability to dissolve salts, PEO and PPO are popular materials for the preparation of polymer electrolytes.[39] Therefore, MD approaches studied how the presence of ions affects the structure and the dynamics of these polymers both in the bulk and in confinement.[37,40–49] Our investigation focuses on the temperature-dependent dynamics of the neat model polymer melts. Specifically, we study the applicability of MCT and the relevance of spatially heterogeneous and cooperative dynamics for the structural relaxation. Moreover, we perform a detailed characterization of the conformational relaxation, elucidating the importance of correlated forward–backward jumps.

II. Methods

The studied PEO and PPO models are comprised of polymer chains, $H-[CH_2-O-CH_2]_{12}-H$ and $CH_3-O-[CH_2-CH(CH_3)-O]_{11}-CH_3$, respectively. Each model is composed of 32 chains. The PPO chains are atactic; i.e., the side groups are randomly connected. The interatomic interactions of these polymer models are described by two well-established quantum-chemistry-based, all-atom force fields,[51,50] which can be written in the form

$$V(\{\mathbf{r}\}) = \sum_{\text{bonds}} V^{\text{bo}}(r_{ij}) + \sum_{\text{angles}} V^{\text{be}}(\theta_{ijk}) + \sum_{\text{dihedrals}} V^{\text{to}}(\varphi_{ijkl}) + V^{\text{nb}}(\{\mathbf{r}\}) \quad (1)$$

Here, $\{\mathbf{r}\}$ is the set of all atomic coordinates. The bonded interactions are comprised of energies due to stretching of bonds, bending of valence angles, and torsion of dihedral angles. The nonbonded interactions V^{nb} are composed of Coulombic and van der Waals interactions, the latter being modeled using a Buckingham potential. The explicit form of the various interaction terms and the corresponding potential parameters are given in the literature.[50–52] In the case of PEO, we apply the force field termed FF-3 in ref 50. It was demonstrated that these models enable a good reproduction of thermodynamic, structural, and dynamical aspects of PEO and PPO melts.[45–47]

The MD simulations were performed using the GROMACS software package.[53] We applied periodic boundary conditions and a time step of 1 fs. The nonbonded interactions were calculated utilizing a cutoff distance of 12 Å. To treat the Coulombic interactions, the particle-mesh Ewald technique was employed.[55] The LINCS algorithm was used to constrain all bonds.[54] Prior to data acquisition, the systems were equilibrated in simulations at constant N, P, and T, using the Rahman-Parrinello barostat[56] and the Nosé-Hoover thermostat.[57] These equilibration runs, which spanned 20−30 ns at the lower temperatures, allowed us to adjust the densities $\rho(T)$. The density increases from $\rho(450\text{ K}) = 1.01$ g/cm^3 to $\rho(280\text{ K}) = 1.12$ g/cm^3 for PEO and from $\rho(450\text{ K}) = 0.89$ g/cm^3 to $\rho(250\text{ K}) = 1.05$ g/cm^3 for PPO. The subsequent production runs were performed in the canonical ensemble, i.e., at constant N, V, and T, employing the Nosé-Hoover thermostat. The trajectories for both systems and all temperatures were saved every 0.5 ps for later analysis. This time interval is sufficiently small so as to resolve the vast majority of the configurational transitions, while the resulting amount of data is still reasonable. Although experimental work demonstrated that PEO is partially crystalline at room temperature and ambient pressure,[39] the simulation results give no evidence for an onset of crystallization in the studied time and temperature ranges.

III. Results

General Characterization of the Structural Relaxation. It is well established for the α relaxation of polymer melts that the time dependence differs from a simple exponential behavior and the temperature dependence does not obey an Arrhenius law.[1] Therefore, we first demonstrate that the studied PEO and PPO models show these key features. While the incoherent intermediate scattering function

$$F_s(q,t) = \langle \cos\{\mathbf{q}\cdot[\mathbf{r}(\tilde{t}_0+t) - \mathbf{r}(\tilde{t}_0)]\}\rangle \quad (2)$$

provides us with information about translational motion, the orientational autocorrelation function

$$F_2(t) = \frac{1}{2}\langle 3[\mathbf{e}(\tilde{t}_0+t)\cdot\mathbf{e}(\tilde{t}_0)]^2 - 1\rangle \quad (3)$$

yields insights into rotational motion. Specifically, the scattering function F_s depends on the translational displacements $[\mathbf{r}(\tilde{t}_0 + t) - \mathbf{r}(\tilde{t}_0)]$ of the atoms during the time interval t, where the absolute value of the scattering vector, $q = |\mathbf{q}|$, determines the length scale on which dynamics is probed. Throughout this contribution, we focus on the translational motion of the oxygen atoms, but we ensured that qualitatively similar findings are obtained for the carbon atoms. The orientational correlation function F_2 depends on the angular displacements $|\mathbf{e}(\tilde{t}_0+t)\cdot\mathbf{e}(\tilde{t}_0)|$ during the time interval t. We study the reorientation of the C−H bonds and $\mathbf{e}(\tilde{t})$ is the unit vector describing the direction of a C−H bond at time $\tilde{t}$. ^{2}H NMR stimulated-echo experiments were used to measure $F_2(t)$ for C−D bonds of deuterated PPO.[58] Mimicking the experimental situation, we restrict the analysis to C−H bonds in the methylene groups to avoid effects from fast 3-fold methyl group jumps. Finally, in eqs 2 and 3, the brackets $\langle ... \rangle$ denote the average over various time origins $\tilde{t}_0$ and over all atoms or bonds belonging to the considered atomic or bond species.

First, we use these correlation functions to ascertain the temperature dependence of the translational and rotational motion associated with the α relaxation. To address the translational aspect, we calculate $F_s(q,t)$ using $q = 1.31$ Å^{-1} and $q = 0.91$ Å^{-1} for PEO and PPO, respectively. These values of the momentum transfer correspond to the respective position of the first maximum of the intermolecular oxygen−oxygen pair distribution functions.[44,45] In Figure 1, we see that the incoherent intermediate scattering functions $F_s(q,t)$ for the oxygen atoms of PPO show a pronounced temperature dependence, in particular at low temperatures. To quantify the slowdown of the structural relaxation, we extract temperature-dependent translational and rotational correlation times according to $F_s(q,\tau_T) = 1/e$ and $F_2(\tau_R) = 1/e$. Figure 2 shows the results for PEO and PPO. For both models, τ_T and τ_R exhibit a comparable temperature dependence that cannot be described by an Arrhenius law, as expected for polymer melts. Rather, a Vogel–Fulcher–Tammann (VFT) law[59]

$$\tau(T) = \tau_\infty \exp\left(\frac{B}{T - T_0}\right) \quad (4)$$

enables good interpolations of the data. VFT fits to τ_T (τ_R) yield $T_0 = 179$ K ($T_0 = 191$ K) for PEO and $T_0 = 179$ K ($T_0 = 175$

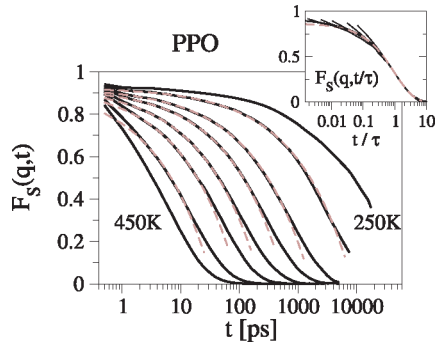

Figure 1. Temperature-dependent incoherent intermediate scattering functions $F_s(q,t)$ for the oxygen atoms of PPO and $q = 0.91$ Å^{-1}. The temperatures are, from left to right, 450, 400, 350, 325, 300, 280, 265, and 250 K. The dashed lines are von Schweidler fits (see eq 9). The inset shows the time–temperature superposition of the same data. The time constants α from KWW interpolations of the α relaxation were used for the scaling of the time axis. The dashed line is a KWW fit of the α relaxation ($\beta = 0.72$).

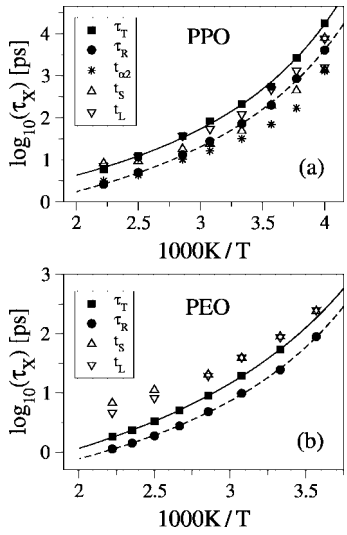

Figure 2. Time constants characterizing the dynamics of the (a) PPO and (b) PEO models. The non-Gaussian parameter α_2, the mean cluster size S_w, and the mean string length L_w are a maximum at $t_{\alpha 2}$, t_s, and t_L, respectively. Moreover, $F_s(q,\tau_T) = 1/e$ and $F_2(\tau_R) = 1/e$. The solid and dashed lines are VFT interpolations of $\tau_T(T)$ (PPO: $T_0 = 179$ K; PEO: $T_0 = 179$ K) and $\tau_R(T)$ (PPO: $T_0 = 175$ K; PEO: $T_0 = 191$ K).

K) for PPO. The results for PPO are in reasonable agreement with $T_0 = 157$–170 K obtained in light scattering and dielectric spectroscopy studies.[60,61]

Inspecting the shape of the scattering functions in Figure 1, we see nonexponential decays. As expected for glass-forming liquids,[1] the time dependence in the α relaxation regime is well described by a Kohlrausch–Williams–Watts (KWW) function, or, equivalently, stretched exponential function

$$F_{KWW}(t) = A \exp\left[-\left(\frac{t}{\tau}\right)^{\beta}\right] \quad (0 \le \beta \le 1) \tag{5}$$

Here, τ and β quantify the time scale and the stretching, respectively. Fitting $F_s(q,t)$ to a KWW function, we find stretching parameters $\beta \approx 0.63$ for PEO and $\beta \approx 0.71$ for PPO, independent of temperature in the studied temperature ranges. For PPO, the time–temperature superposition is further demonstrated in the inset of Figure 1. Clearly, the curves coincide in the α relaxation regime when the time axis is scaled with the correlation time τ. KWW interpolations of $F_2(t)$ yield stretching parameters $\beta \approx 0.36$ for PEO and $\beta \approx 0.48$ for PPO, consistent with stretching parameters obtained from ^{2}H NMR stimulated-echo experiments near T_g.[58] Thus, with respect to both temperature and time dependence, the structural relaxation of the studied polymer models resembles that of PEO and PPO melts, confirming the quality of the used force fields.[46]

We note that, for PPO at $T = 250$ K, the translational and rotational correlation functions give evidence for some deviations from time–temperature superposition in the early stages of the decay, where the curves decrease significantly faster than expected from the KWW behavior (see Figure 1). Since dielectric spectroscopy studies demonstrated that PPO exhibits a Johari−Goldstein secondary relaxation, which starts to separate from the primary relaxation at $T \approx 250$ K,[60–62] we tentatively attribute these deviations to the onset of this secondary process.

B. MCT Analysis. The time–temperature superposition observed for the α relaxation of the PEO and PPO models is in agreement with MCT.[9] Therefore, we now check whether further predictions of this theory are fulfilled. According to MCT, the particles of glass-forming liquids are trapped in cages formed by their neighbors for some time until an escape from these cages is possible during the structural relaxation. As a consequence of this trapping, a plateau regime or, equivalently, β relaxation regime, preceding the α relaxation regime develops when the temperature is decreased toward the critical temperature T_c. Quantitatively, MCT predicts a power-law divergence of the α relaxation time at the critical temperature T_c:

$$\tau(T) \propto (T - T_c)^{-\gamma} \tag{6}$$

Another key prediction of MCT is the factorization theorem for the β relaxation regime. It states that, for such times, all correlation functions, in particular, the incoherent intermediate scattering functions for different values of the momentum transfer, can be written as

$$F_s(q,t) = f_q^c + a_q G(t) \tag{7}$$

Here, the plateau value f_q^c and the amplitude a_q depend on the value of q, while the β correlator $G(t)$ is independent of the observable. If the factorization theorem is obeyed, the curves

$$R(q,t) = \frac{F_s(q,t) - F_s(q,t')}{F_s(q,t'') - F_s(q,t')} \tag{8}$$

for different values of the momentum transfer will collapse onto a master curve, provided the times t' and t'' are chosen inside the β relaxation regime.[63] Hence, calculation of $R(q,t)$ allows one to check the factorization theorem without invoking a fitting procedure. $G(t)$ can be expanded for times close to the central β relaxation time t_σ. The expansion for $t > t_\sigma$ leads to the von Schweidler law

$$F_s(q,t) = f_q^c - h_q t^b \tag{9}$$

showing that a power law characterized by the universal von Schweidler exponent b describes the initial stages of the decay from the plateau. For temperatures $T > T_c$, the amplitude h_q decreases upon cooling according to

$$h_q(T) \propto (T - T_c)^{\gamma b} \tag{10}$$

Finally, within MCT, b and γ are related via the exponent parameter λ:

$$\lambda = \frac{\Gamma^2(1-a)}{\Gamma(1-2a)} = \frac{\Gamma^2(1+b)}{\Gamma(1+2b)}, \quad \gamma = \frac{1}{2a} + \frac{1}{2b} \tag{11}$$

To check these MCT predictions for the PPO model, we analyze the scattering functions $F_s(q,t)$ of the oxygen atoms for various values of the momentum transfer q. First, we fit a KWW function to the scattering functions in the α relaxation regime. Figure 3a shows the temperature-dependent correlation times

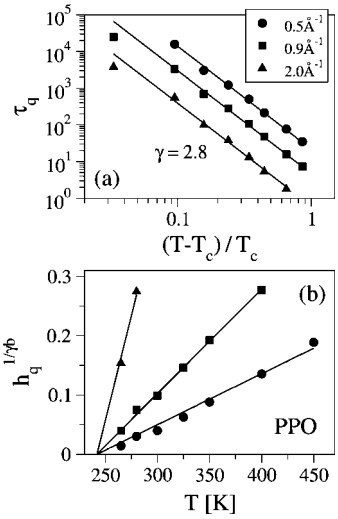

Figure 3. Test of MCT predictions for PPO on the basis of the incoherent intermediate scattering functions $F_s(q,t)$ of the oxygen atoms. (a) Correlation times τ_q resulting from KWW fits of the α relaxation regime for the indicated values of q. The solid lines are MCT power laws $\tau_q \propto (T - T_c)^{-\gamma}$ where $T_c = 242$ K and $\gamma = 2.8$. (b) Temperature dependence of $h_q^{1/\gamma b}$, using $\gamma b = 1.44$ for $q = 0.50$ Å^{-1}, $\gamma b = 1.34$ for $q = 0.91$ Å^{-1}, and $\gamma b = 1.16$ for $q = 2.00$ Å^{-1}. The solid lines are linear interpolations $h_q^{1/\gamma b} \propto (T - 242$ K).

τ_q resulting from these fits for three values of q. A MCT power law (see eq 6) with $T_c = 242 \pm 2$ K and $\gamma = 2.8 \pm 0.1$ nicely describes all data at $T/T_c - 1 \geq 0.1$. These findings are in reasonable agrement with $T_c = 236 \pm 2$ K and $\gamma = 3.7 \pm 0.8$ from experimental studies.[60,64] However, there are deviations from the MCT power law at the lowest temperature $T/T_c - 1 \approx 0.03$. At the present, it is not clear whether these deviations are related to the possible onset of the Johari−Goldstein secondary relaxation near T_c. Qualitatively similar deviations from the MCT predictions were reported for a chemically realistic model of polybutadiene in the vicinity of the critical temperature.[13]

Next, we fit the von Schweidler law to the scattering functions $F_s(q,t)$. Because of a possible interference of the Johari−Goldstein secondary relaxation, we exclude the data for the lowest temperature $T = 250$ K from further MCT analysis. The von Schweidler law enables a good interpolation of the decays in the late-β/early-α relaxation regime (see Figure 1). For $q = 0.91$ Å^{-1}, the von Schweidler fits yield $f_q^c = 0.93 \pm 0.01$ and $b = 0.46 \pm 0.01$ independent of temperature. According to eq 11, this value of the von Schweidler exponent b translates into $\gamma = 2.9$, in agreement with $\gamma = 2.8 \pm 0.1$ determined from the temperature-dependent correlation times τ_q. To check the validity of eq 10, we use the exponents $b = 0.46$ and $\gamma = 2.9$ and plot the temperature dependence of $h_q^{1/\gamma b}$ in Figure 3b. In harmony with the MCT prediction, there is a linear relationship, and by extrapolation, $h_q^{1/\gamma b}$ vanishes at the critical temperature $T_c = 242$ K, extracted from the temperature dependence of the α relaxation.

However, the MCT predictions are not fulfilled when including the scattering functions for other values of q into the analysis. Von Schweidler fits for $q = 0.5$ Å^{-1} and $q = 2.0$ Å^{-1} yield $b = 0.59 \pm 0.02$ and $b = 0.23 \pm 0.02$, respectively, corresponding to $\gamma = 2.4$ and $\gamma = 5.0$. Thus, there is no universal von Schweidler exponent, and for high and low values of q, the values of γ calculated from the von Schweidler exponents deviate from $\gamma = 2.8$, resulting from the temperature dependence of the α relaxation. To demonstrate the violation of the factorization theorem independent of any fitting routine, we show $R(q,t)$ for different values q in Figure 4. The data were

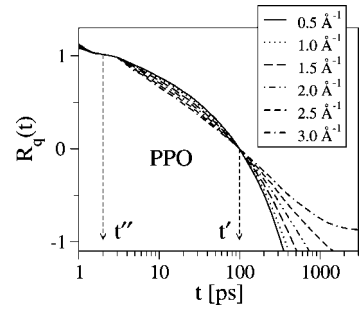

Figure 4. Test of the MCT factorization theorem for PPO at $T = 265$ K. The functions $R(q,t)$ were obtained from the data $F_s(q,t)$ for the oxygen atoms according to eq 8. The values of the momentum transfer q are indicated, and times $t'' = 2$ ps and $t' = 100$ ps were used.

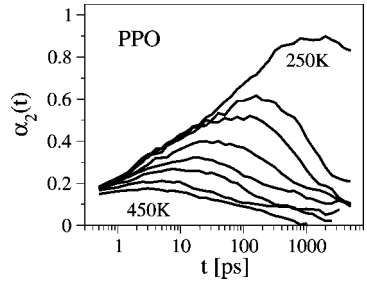

Figure 5. Non-Gaussian parameter $\alpha_2(t)$ for the oxygen atoms of PPO at various temperatures (450, 400, 350, 325, 300, 280 265, and 250 K).

calculated from $F_s(q,t)$ for the oxygen atoms of PPO at $T = 265$ K. Clearly, the data do not collapse onto a master curve in the β relaxation regime, indicating the violation of the factorization theorem. Qualitatively similar results were observed at all studied temperatures.

C. Spatially Heterogeneous Dynamics. Other models of the glass transition focus on the heterogeneity and the cooperativity of the dynamics.[14,15] The importance of these effects was demonstrated in MD simulation studies on various glass-forming liquids.[22–36] Here, we investigate the relevance of heterogeneity and cooperativity for the first time for chemically realistic polymer models. For various model-glass formers, it was found that the distribution of scalar particle displacements $|\mathbf{r}(\tilde{t}_0 + t) - \mathbf{r}(\tilde{t}_0)|$ deviates from a Gaussian at intermediate times t between ballistic and diffusive motion. These deviations, which are a first indication for the existence of heterogeneous dynamics, can be quantified by the non-Gaussian parameter

$$\alpha_2(t) = \frac{3}{5}\frac{\langle[\mathbf{r}(\tilde{t}_0 + t) - \mathbf{r}(\tilde{t}_0)]^4\rangle}{\langle[\mathbf{r}(\tilde{t}_0 + t) - \mathbf{r}(\tilde{t}_0)]^2\rangle^2} - 1 \qquad (12)$$

Figure 5 shows $\alpha_2(t)$ for the oxygen atoms of PPO at various temperatures. We see that the non-Gaussian parameter exhibits a maximum in the late-β/early-α relaxation regime, consistent with findings for various model-glass formers.[22,31–33,35] When the temperature is decreased, the position of the maximum, $t_{\alpha 2}$, shifts to longer times. In Figure 2a, we see that the temperature dependence of $t_{\alpha 2}$ is somewhat weaker, but still comparable to that of the α relaxation time. The maximum $\alpha_2(t_{\alpha 2})$ increases upon cooling, in particular near the critical temperature T_c, but the values are relatively small. More precisely, at comparable temperatures near T_c, $\alpha_2(t_{\alpha 2}) = 1.3$–$2.5$ was reported for the other studied models of glass-forming liquids, except for the silicon atoms in silica showing $\alpha_2(t_{\alpha 2}) = 0.8$ (see ref 35 for a detailed comparison). For PEO, the non-Gaussian parameter is even smaller than for PPO. This results in some ambiguities when extracting the maximum positions so that we refrain from discussing the temperature dependence of $t_{\alpha 2}$ for PEO.

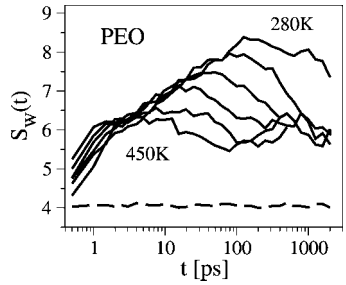

Figure 6. Mean cluster size $S_w(t)$ of highly mobile oxygen atoms for PEO at temperatures 450, 400, 350, 325, 300, and 280 K. When the particles used for the analysis are chosen irrespective of their mobilities, a mean cluster size of $S_w \simeq 4$ results, as indicated by the dashed line.

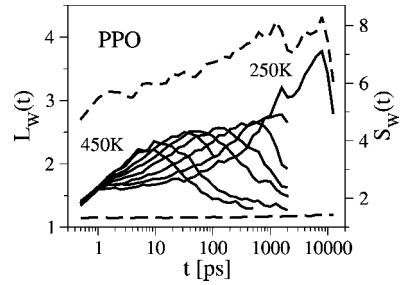

Figure 7. Mean string length $L_w(t)$ of highly mobile oxygen atoms for PPO at temperatures 450, 400, 350, 325, 300, 280, 265, and 250 K. When the oxygen atoms used for the analysis are chosen irrespective of their mobilities, a mean string length of $L_w \simeq 1.1$ results, as indicated by the bottom-most dashed line. The up-most dashed line is the mean cluster size $S_w(t)$ of highly mobile oxygen atoms for PPO at $T = 250$ K.

To ascertain the spatial heterogeneity of the PEO and PPO dynamics, we demonstrate that highly mobile oxygen atoms form clusters larger than expected from random statistics. Following previous studies,[25,28,29,33,35] we characterize the particle mobility in a time interval t by the scalar displacement and select the 5% most mobile oxygen atoms for further analysis. Then, we define a cluster as a group of the most mobile oxygen atoms that reside in the first neighbor shells of each other. For both polymers, we use the position of the first minimum of the respective intermolecular oxygen−oxygen pair distribution function as criterion for the extension of the neighbor shell. On the basis of the probability distribution $p_s(n,t)$ of finding a cluster of size n for a time interval t, we calculate the weight-averaged mean cluster size

$$S_w(t) = \frac{\sum_n n^2 p_s(n,t)}{\sum_n n p_s(n,t)} \tag{13}$$

This quantity measures the average size of a cluster to which one of the most mobile oxygen atoms belongs. Previously, it was shown that the conclusions resulting from such analysis are unchanged when the fraction of highly mobile particles is varied in a meaningful range.[35]

The mean cluster size $S_w(t)$ is displayed for PEO at various temperatures in Figure 6. It is evident that $S_w(t)$ shows a maximum, which increases upon cooling. By contrast, a time and temperature independent small size $S_w \approx 4$ characterizes the clusters for the case of random statistics, i.e., when 5% of the oxygen atoms are chosen for analysis irrespective of their mobilities. These results clearly demonstrate the existence of spatially heterogeneous dynamics. The transient nature of the clusters can be quantified, when we determine the times t_S at which $S_w(t)$ is a maximum. In Figure 2, we see for PEO and PPO that the clusters are largest in the α relaxation regime at all studied temperatures. For PPO, we observe that the single maximum of $S_w(t)$ at high temperatures splits into two peaks near T_c (see Figure 7). This can be taken as another hint that a primary and a secondary relaxation coexist at sufficiently low temperatures.

In Figure 6, a closer inspection of the data for the highest temperatures reveals that $S_w(t)$ increases at long times in the diffusive regime. This increase is the mere consequence of the chain connectivity. At sufficiently long times, the displacements of the individual atoms are largely determined by the displacement of the center-of-mass of the respective polymer chain, and hence, those oxygen atoms are highly mobile that belong to chains, showing the largest center-of-mass displacements from the statistical distribution. Because of their spatial proximity along the chain, these atoms form extended clusters so that $S_w(t)$ increases when the single particle displacements start to become dominated by the center-of-mass displacements. By contrast, the maximum at shorter times is not due to chain connectivity.

It has been shown that cooperative stringlike motion is an important channel for the relaxation of highly mobile particles in simple model-glass formers.[25,29−31] Therefore, we investigate the relevance of stringlike motion for the chemically realistic PEO and PPO models. Following these previous studies, we construct strings by connecting any two oxygen atoms i and j if the condition

$$\min[|\mathbf{r}_i(\tilde{t}_0) - \mathbf{r}_j(\tilde{t}_0 + t)|,\ |\mathbf{r}_j(\tilde{t}_0) - \mathbf{r}_i(\tilde{t}_0 + t)|] < \delta$$

holds for the atomic positions at two different times and set δ to about 55% of the intermolecular oxygen−oxygen distance, i.e., $\delta = 0.27$ nm for PEO and $\delta = 0.38$ nm for PPO. Then, this condition means that one oxygen atom has moved and an another oxygen atom has occupied its position. We checked that our conclusions are not altered when δ is varied in a meaningful range. Using the above criterion, we determine the probability $p_l(l,t)$ of finding a string of length l for a time interval t and calculate the weight-averaged mean string length $L_w(t)$ in analogy with eq 13.

Figure 7 shows $L_w(t)$ for PPO at various temperatures. Evidently, the strings grow and shrink in time and they are substantially longer than that resulting from random statistics. Upon cooling, the position of the maximum, t_L, shifts to longer times and the height of the maximum increases, where the growth is particularly prominent in the vicinity of T_c. Thus, stringlike motion is an important phenomenon at sufficiently low temperatures. $L_w(t)$ and $S_w(t)$ show a similar behavior. In particular, both quantities exhibit a two-peak signature at $T = 250$ K. The temperature dependence of t_L and t_S is compared in Figure 2. For PEO and PPO, the strings, like the clusters, are largest in the α relaxation regime. By contrast, simulation studies on simple glass-forming liquids, including a bead−spring polymer model, found that t_L and t_S are located in the late-β/early-α relaxation regime, i.e., at significantly shorter times.[25,28−31,33,35] We conclude that the PEO and PPO models do show spatially heterogeneous and cooperative dynamics; however, the characteristics of these effects differ from that for simple model-glass formers.

D. Conformational Relaxation. Local conformational dynamics are of central importance for the structural relaxation of polymers.[5] In the following, we investigate the torsional motion of the PEO model by analyzing the angular trajectories $\phi_{cc}(\tilde{t})$ and $\phi_{oc}(\tilde{t})$, describing the time evolution of the OCCO and COCC dihedral angles, respectively. Figure 8 presents a typical trajectory $\phi_{cc}(\tilde{t})$. Comparison with the probability distribution of the dihedral angle, $p(\phi_{cc})$, shows that the torsional motion is comprised of well-defined transitions between the

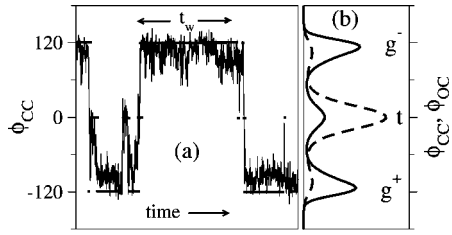

Figure 8. Results for PEO at $T = 280$ K. (a) Typical trajectory $\phi_{cc}(\tilde{t})$ of an OCCO dihedral angle during a time interval of 1.15 ns. The straight lines mark the discontinuous trajectory $s_{cc}(\tilde{t})$ resulting from mapping of the trajectory $\phi_{cc}(\tilde{t})$ onto the conformational states g^-, t, and g^+. (b) Probability distributions of the OCCO (solid line) and COCC (dashed line) dihedral angles, $p(\phi_{cc})$ and $p(\phi_{oc})$, respectively.

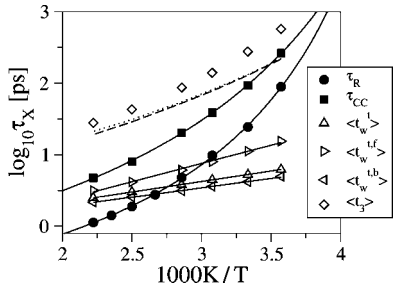

Figure 9. Time constants characterizing the conformational dynamics of the OCCO dihedrals in the PEO model. We show the torsional correlation times τ_{cc}, defined as $P_{cc}(\tau_{cc}) = 1/e$, and the rotational correlation times τ_R, see Figure 2, together with VFT interpolations. Moreover, the mean waiting times of the OCCO dihedrals in the t state are displayed. While all escape processes from the t state are considered for the calculation of $\langle t_w^t \rangle$, $\langle t_w^{t,f} \rangle$ ($\langle t_w^{t,b} \rangle$) characterizes explicitly the forward (backward) jumps $g^{\pm} \rightarrow t \rightarrow g^{\mp}$ ($g^{\pm} \rightarrow t \rightarrow g^{\mp}$). The solid lines are Arrhenius fits ($\langle t_w^t \rangle$: $E_a = 0.025$ eV, $\langle t_w^{t,f} \rangle$: $E_a = 0.044$ eV, $\langle t_w^{t,b} \rangle$: $E_a = 0.023$ eV). Finally, we present the mean times $\langle t_3 \rangle$ needed for an OCCO dihedral to visit each of the three conformational states at least once. Calculated values of $\langle t_3 \rangle$ are shown as dotted and dashed lines. While $g^{\pm} \leftrightarrow g^{\mp}$ transitions were neglected when calculating the former data, these transitions were taken into account when computing the latter data; see text for details.

gauche$^-$ (g^-), *trans* (t), and *gauche*$^+$ (g^+) states, suggesting that a discretization is useful for an analysis of the conformational dynamics. Therefore, we map the trajectories $\phi_x(\tilde{t})$ onto discrete sequences $s_x(\tilde{t})$ of the conformational states (see Figure 8). In this way, we eliminate effects from librational motions, which do not lead to structural relaxation. Then, analysis of the discrete sequences $s_x(\tilde{t})$ enables a straightforward characterization of the relevant torsional motion, e.g., in terms of waiting times t_w and back-jump probabilities p_b (see below).

To study the time scale of the conformational relaxation, we use the discrete sequences s_x and determine the probabilities $p_x(t)$ of finding a dihedral in the same conformational state at two times separated by a time interval t. Because of the finite number of conformational states, these probabilities exhibit a finite and temperature-dependent plateau value $p_x(\infty)$. To remove this effect, we calculate the torsional correlation functions

$$P_x(t) = \frac{\langle p_x(t) \rangle - \langle p_x(\infty) \rangle}{1 - \langle p_x(\infty) \rangle} \tag{14}$$

and determine torsional correlation times τ_x according to $P_x(\tau_x) = 1/e$. In Figure 9, we compare the torsional correlation time τ_{cc} with the rotational correlation time τ_R, characterizing the reorientation of the C−H bond vectors. We see that both time constants show a comparable temperature dependence, implying that the conformational and the structural relaxations are related, consistent with results for other polymer models.[5,65] Some deviations in the temperature dependence are expected since, in particular at high temperatures, librational motions affect the rotational correlation times more than the torsional correlation times obtained from analysis of the discrete jump sequences. Moreover, the conformational dynamics of several dihedral species render the orientation of a given C−H bond time dependent, and hence, the absolute values of the rotational and torsional correlation times should differ.

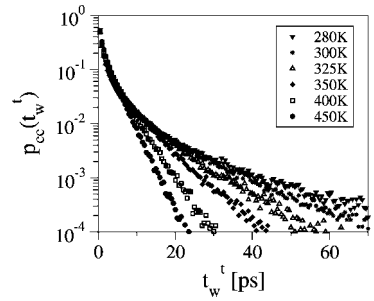

Figure 10. Probability distributions $p_{cc}(t_w^t)$ characterizing the waiting times of the OCCO dihedrals in the t state. Results for PEO at various temperatures are compared.

Next, we study the waiting times t_w in the conformational states, i.e., the time intervals between two subsequent conformational transitions. We find that the waiting times differ between the OCCO and COCC dihedral angles, and for each dihedral species, they depend on the conformational state. Therefore, we separately determine the waiting times for each dihedral species and conformational state. The temperature-dependent mean waiting time of the OCCO dihedrals in the t state, $\langle t_w^t \rangle$, is included in Figure 9. We see that the mean waiting time follows an Arrhenius law with a small activation energy $E_a = 0.025$ eV. Qualitatively similar results are observed for all other dihedral species and conformational states. Hence, the temperature dependence of the mean waiting times is much weaker than that of the rotational and torsional correlation times, indicating that the longer residence times in the conformational states at lower temperatures are not sufficient to explain the strong slowdown of the α relaxation upon cooling, in harmony with results for other all-atom polymer models.[5]

Closer insights into the nature of the conformational dynamics are available from the probability distributions of the waiting times, $p_x(t_w)$. Figure 10 shows the distributions $p_{cc}(t_w^t)$, which characterize the waiting times of the OCCO dihedrals in the t state. In particular, at the lower temperatures, there are substantial deviations from an exponential waiting-time distribution, indicating that a Markov process does not apply to the conformational dynamics. At short waiting times, we see a nonexponential decay, which exhibits a weak temperature dependence. At long waiting times, there is a nearly exponential and more temperature-dependent decay. Qualitatively similar waiting-time distributions are observed for all dihedral species and conformational states, suggesting that the distributions are comprised of two contributions governing the behavior at short and long waiting times, respectively.

In general, one can distinguish between forward and backward jumps. Let $\sigma_{i-1} \rightarrow \sigma_i \rightarrow \sigma_{i+1}$ be a sequence of three subsequently visited conformational states. Then, a forward and a backward jump in the state σ_i are associated with $\sigma_{i-1} \neq \sigma_{i+1}$ and $\sigma_{i-1} = \sigma_{i+1}$, respectively. Unlike backward jumps, forward jumps enable visiting all three conformational states, and hence, they may be the cornerstone of conformational relaxation. Since transitions $g^{\pm} \rightarrow g^{\mp}$ are rare for the OCCO and COCC dihedrals at the studied temperatures, the behavior in the t state is of particular importance for the exploration of all conformational states. Figure 11 shows the probability distributions $p_x(t_w^t)$ characterizing the waiting times in the t state during the forward

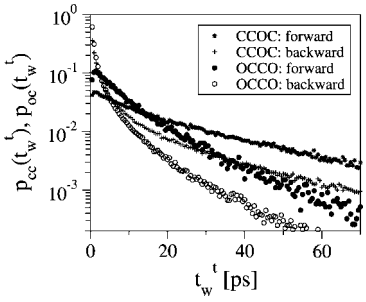

Figure 11. Probability distributions $p_{cc}(t_w^t)$ and $p_{oc}(t_w^t)$ characterizing the waiting times of the OCCO and COCC dihedrals in the t state, respectively. Results for PEO at $T = 300$ K are shown. For both dihedral species, we distinguish the waiting times prior to a forward jump ($g^{\pm} \rightarrow t \rightarrow g^{\mp}$) from that prior to a backward jump ($g^{\pm} \rightarrow t \rightarrow g^{\pm}$).

($g^{\pm} \rightarrow t \rightarrow g^{\mp}$) and backward ($g^{\pm} \rightarrow t \rightarrow g^{\pm}$) sequences, respectively. We see that the results for the two dihedral species are comparable. Thus, it is not important that the t state is the majority state of ϕ_{oc}, whereas it is the minority state of ϕ_{cc} (see Figure 8). However, the waiting times strongly depend on the direction of the jumps. For both dihedral species, the forward jumps are characterized by nearly exponential waiting-time distributions, and hence, the propensity to perform such transition does not depend on the jump history. The backward jumps exhibit a more complex behavior. In a semilogarithmic representation, the slope of the curves decreases with increasing waiting time until it becomes constant, indicative of an exponential behavior at sufficiently long waiting times. In the latter regime, the slope is comparable for the forward and backward jumps.

These findings imply that both uncorrelated and correlated conformational transitions occur. In some cases, the time and the direction of a jump are independent of the history, resulting in an exponential behavior and in similar rates of forward and backward jumps. In other cases, the dihedrals have a high tendency to return to the previous conformational state almost immediately, i.e., to perform a correlated backward jump, leading to the observed nonexponentiality at short waiting times. One can imagine that this proneness to a correlated backward jump depends on the jump history. For example, it may become weaker when time elapses after the previous transition. Also, a correlated backward jump may be less likely when a large number of forward–backward jumps have already taken place, i.e., when previous "unsuccessful" attempts have paved the way for a "successful" transition to a new state (see below).

To further investigate the role of the forward jumps for the conformational and structural relaxations, we analyze their temperature-dependent behavior. Figure 12 shows the distributions $p_{cc}(t_w^t)$ characterizing the waiting times of the OCCO dihedrals in the t state prior to a forward jump at various temperatures. Evidently, all waiting-time distributions are nearly exponential, confirming that the point in time of a forward jump is independent of the history. In Figure 9, we compare the temperature-dependent mean waiting times $\langle t_w^{f,t} \rangle$ and $\langle t_w^{b,t} \rangle$ characterizing the forward and the backward jumps in the t state, respectively. We see that the forward jumps exhibit a higher temperature dependence than the backward jumps. Specifically, the activation energies amount to $E_a = 0.044$ eV for the former and $E_a = 0.023$ eV for the latter. For comparison, when the two adjacent COCC dihedrals are fixed in the t state, the used force field yields an energy barrier, including Coulombic contributions, of about 0.05 eV against $g^{\pm} \leftrightarrow t$ transitions of an OCCO dihedral,[47] which is in good agreement with the observed activation energy for the forward jumps. However, the temperature dependence of $\langle t_w^{f,t} \rangle$ is still much weaker than that of the torsional and rotational correlation times, corroborating our previous conclusion that the longer waiting times at lower temperatures do not provide an explanation for the slowdown of the α relaxation upon cooling.

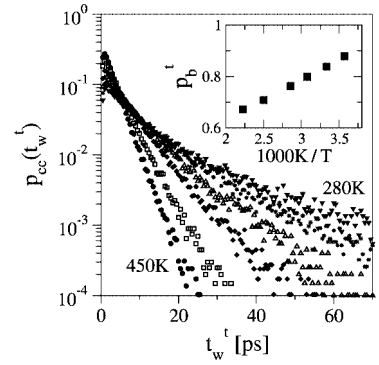

Figure 12. Probability distribution $p_{cc}(t_w^t)$ characterizing the waiting times of the OCCO dihedrals in the t state prior to a forward jump. Results for PEO at various temperatures are shown. The inset displays the temperature dependence of the probability p_b^t that a forward jump $g^{\pm} \rightarrow t$ is followed by a direct backward jump $t \rightarrow g^{\pm}$ to the initial dihedral state.

These findings show that it is not sufficient to study single events, but it is necessary to correlate the times and the directions of two or more conformational transitions. First, we analyze the directions of two consecutive jumps. Specifically, we determine the back-jump probability p_b^t in the t state, i.e., the probability that a transition $g^{\pm} \rightarrow t$ is followed by a transition $t \rightarrow g^{\pm}$. In Figure 12, the temperature-dependent back-jump probabilities p_b^t of the OCCO dihedrals are presented. We see a substantial increase of p_b^t upon cooling. Thus, when the temperature is decreased, both longer waiting times and higher back-jump probabilities contribute to the slower exploration of the conformational states. In other words, the increase of the back-jump probabilities leads to an additional delay of the conformational relaxation and, hence, to deviations from an Arrhenius behavior. We note that, for a determination of meaningful back-jump probabilities, it is important that the time interval $\Delta\tilde{t}$ between two consecutive configurations of the trajectory is small with respect to the waiting times, in particular with respect to the short periods prior to backward jumps. Here, we use a time interval of 0.5 ps resulting in ratios $\langle t_w^{b,t} \rangle / \Delta\tilde{t} = 4-10$ in the studied temperature range. When we redo the analysis for $T = 280$ K utilizing $\Delta\tilde{t} = 1.0$ ps rather than $\Delta\tilde{t} = 0.5$ ps so that the ratio $\langle t_w^{b,t} \rangle / \Delta\tilde{t}$ is comparable at the highest and lowest studied temperatures, the back-jump probability decreases from $p_b^t = 0.88$ to $p_b^t = 0.85$. Hence, the back-jump probability at $T = 280$ K is still substantially higher than $p_b^t = 0.67$ at $T = 450$ K, indicating that our conclusions are not affected when the time interval $\Delta\tilde{t}$ is varied in a reasonable range.

To study the exploration of the dihedral states in more detail, we determine the times t_3 needed for the dihedrals to visit all three conformational states. Specifically, we start from a randomly chosen time origin and define t_3 as the time elapsing until a given dihedral has first visited each of the three conformational states at least once. In Figure 8, we include the mean times $\langle t_3 \rangle$ resulting from the conformational dynamics of the OCCO dihedrals at various temperatures. Unlike the mean waiting times, the exploration times $\langle t_3 \rangle$ do not follow an Arrhenius law. However, their temperature dependence is still weaker than that of the torsional correlation times, implying that the relation between the exploration process and the conformational relaxation is not straightforward, but subtle. We note that previous work on polybutadiene did not relate the exploration process to the primary, but rather to the secondary relaxation.[7]

The question arises whether knowledge of the back-jump probabilities and of the mean waiting times prior to forward and backward jumps is sufficient to calculate the exploration times. To tackle this question, we assume that, at the randomly chosen time origin, an OCCO dihedral occupies one of the *gauche* states, being the majority states, and calculate the average time needed for the dihedral to visit each conformational state at least once. First, we neglect direct transitions between the *gauche* states due to their rareness. Then, a forward jump in the t state is necessary to visit all dihedral states. Prior to a forward jump, the OCCO dihedral can perform n_{bj} backward jumps in the t state. Thus, in general, sequences $g^{\pm} \rightarrow n_{bj}(t \rightarrow g^{\pm} \rightarrow)\, t \rightarrow g^{\mp}$ lead to the exploration of all conformational states. Provided the back-jump probability in the t state is independent of the history, the probability of finding a sequence with n_{bj} backward jumps in the t state is given by $(1 - p_b^t)(p_b^t)^{n_{bj}}$. Then, the average time $\langle t_{gtg} \rangle$ to move from one of the *gauche* states to the other can be written as

$$\langle t_{gtg} \rangle = (1 - p_b^t) \sum_{n_{bj}=0} (p_b^t)^{n_{bj}} (t_{fl} + n_{bj} t_{bf}) = t_{fl} + \frac{p_b^t}{1 - p_b^t} t_{bf} \tag{15}$$

Here, t_{bf} is the time needed for a forward–backward jump sequence and t_{fl} is the sum of the times elapsing prior to the first and the last conformational transition. When we assume that the waiting times can depend on the jump direction, but are otherwise independent of the history, t_{bf} and t_{fl} are determined by the mean waiting times $\langle t_w^{t,f} \rangle$ and $\langle t_w^{t,b} \rangle$ and by the mean waiting time $\langle t_w^g \rangle$ in the $g^{\pm}$ states, which is found to be essentially independent of the jump direction. Specifically, $t_{bf} = \langle t_w^{t,b} \rangle + \langle t_w^g \rangle$ and $t_{fl} = \langle t_w^g/2 \rangle + \langle t_w^{t,f} \rangle$. The factor 1/2 in the latter equation is a consequence of the fact that, on average, the randomly chosen time origin lies in the middle of the waiting time before the first jump.

Utilizing the knowledge of the mean waiting times and of the back-jump probabilities, we calculate the times $\langle t_{gtg} \rangle$ according to eq 15. In Figure 8, we see that the temperature dependence of $\langle t_{gtg} \rangle$ deviates from an Arrhenius law due to the higher back-jump probabilities at lower temperatures. While the calculated and the actual exploration times are similar at high temperatures, the former show a weaker temperature dependence. Therefore, we dropped the assumption that direct transitions between the *gauche* states can be neglected and recalculated the mean times $\langle t_{gtg} \rangle$. In Figure 8, it is evident that considering the transitions between the *gauche* states has hardly any effect. Therefore, we refrain from specifying the equations for this case. Also, we expect that the assumption to start in one of the *gauche* states is not crucial, in particular at low temperatures, where the occupation of the *trans* state is small. The deviations between the calculated and the actual exploration times rather show that the assumption of history independent waiting times and back-jump probabilities is not justified, further illustrating the complexity of the conformational dynamics.

Finally, we analyze the torsional motion of the OCCO dihedrals on a longer time scale $t \approx 10\langle t_w \rangle$, where $\langle t_w \rangle$ is the mean waiting time resulting from all conformational transitions of this dihedral species. We calculate the probability distribution $z_{cc}(n,t)$ of finding n conformational transitions during a time interval t. Figure 13 shows the distributions $z_{cc}(n,t)$ obtained for $t \approx 10\langle t_w \rangle$ at $T = 280$ K and $T = 450$ K. The data for the higher temperature resemble the Poisson distribution for the used ratio $t/\langle t_w \rangle \approx 10$, and hence, a Markov process approximates the conformational dynamics. By contrast, substantial deviations from the Poisson distribution are obvious for the lower temperature. Specifically, $z_{cc}(n,t)$ is much broader, indicating that a large fraction of dihedrals performs less or more transitions than expected for the case of uncorrelated jump events. Thus, at sufficiently low temperatures, pronounced dynamical heterogeneities do govern not only the structural relaxation (see section III.C) but also the conformational relaxation.

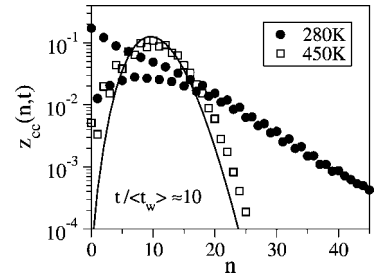

Figure 13. Probability $z_{cc}(n,t)$ of finding n conformational transitions of the OCCO dihedrals during a time interval t. We used $t = 125.5$ ps and $t = 39.5$ ps for PEO at $T = 280$ K ($\langle t_w \rangle = 14.3$ ps) and $T = 450$ K ($\langle t_w \rangle = 3.9$ ps), respectively. Thus, the ratio between the time interval and the mean waiting time amounts to $t/t_w \simeq 10$ for both temperatures. The solid line is the Poisson distribution calculated using the values of t and t_w at $T = 450$ K, i.e., $t/t_w = 10.1$.

Furthermore, it is evident from Figure 12 that it is more probable to find an even than an uneven number of conformational transitions in a given time interval. This effect, which is most pronounced for small n and low temperatures, is another consequence of the existence of correlated forward–backward jumps. It implies that, at a given time, each OCCO dihedral has a preferred conformational state. After the exit of its preferred state, a dihedral tends to return to this state within a very short period of time performing a correlated backward jump. Then, on average, the dihedrals spend much longer times in the preferred state than in the unpreferred state of the forward–backward sequence, resulting in a higher probability of finding an even number of jumps, consistent with the observation. At $T = 280$ K, the difference between even and uneven n is small for $n > 30$, and hence, the information about the preferred state vanishes after about 30 conformational transitions, i.e., after about 15 forward–backward jump sequences.

E. Conclusions. We have performed MD simulations to investigate the translational and rotational motion of chemically realistic polymer models. For the studied PEO and PPO models, the structural relaxation shows the typical properties of polymer melts; i.e., its time dependence differs from a single-exponential function, and its temperature dependence deviates from an Arrhenius law, in harmony with results in the literature.[47] Specifically, for both polymer models, a KWW function well interpolates the translational and rotational correlation functions in the α relaxation regime, time–temperature superposition is obeyed, and a VFT law describes the temperature-dependent α relaxation times. The stretching and the temperature dependence of the correlation functions are consistent with results from experimental work, confirming the quality of the used force fields.

Recently, the applicability of MCT to the structural relaxation of chemically realistic polymer models was controversially discussed.[5,8,12,13] Here, we have performed a MCT analysis for the PPO model using the incoherent intermediate scattering functions of the oxygen atoms. On the one hand, the analysis shows that a MCT power law with a critical temperature $T_c = 242 \pm 2$ K well describes the temperature-dependent correlation times in the range $(T - T_c)/T_c = 0.1-0.9$. Also, for a momentum transfer q corresponding to the intermolecular oxygen−oxygen distance, further MCT predictions are fulfilled. On the other hand, the temperature dependence of the α relaxation time deviates from a MCT power law in the immediate vicinity of T_c, and the factorization theorem, being a central MCT predic-

tion for the α relaxation regime, is violated. We conclude that MCT captures several aspects of the structural relaxation at appropriate temperatures and length scales; however, it does not provide a complete description since energy barriers against the torsional motion affect the dynamical behavior.

Furthermore, we have studied the heterogeneity and the cooperativity of the structural relaxation. For the PEO and PPO models, we have demonstrated that highly mobile oxygen atoms aggregate into transient clusters, indicating the spatially heterogeneous nature of the dynamics. Furthermore, we have shown that cooperative stringlike motion facilitates the translational displacements of the highly mobile oxygen atoms at intermediate times between ballistic motion and diffusive motion. Both clusters and strings increase in size upon cooling, and hence, spatial heterogeneity and cooperativity are prominent aspects of the molecular dynamics in particular at low temperatures, in harmony with results for various models of glass-forming liquids.[3] Concerning the transient nature of these phenomena, we have found that the mean cluster size S_w and the mean string length L_w are a maximum at comparable times $t_s \simeq t_L$ in the α relaxation regime for PEO and PPO. In this respect, the present findings differ from previous results. Specifically, the clusters and the strings were reported to be largest at significantly earlier times in the late-β/early-α relaxation regime for models of atomic liquids,[25,29] water,[33] silica,[34,35] and a bead−spring polymer.[28,31] We conclude that the existence of spatially heterogeneous and cooperative dynamics is common to a broad variety of glass-forming liquids. However, the characteristics of these phenomena differ among the materials, and hence, relating the properties of the heterogeneity and the cooperativity of the molecular dynamics to the respective features of the structural relaxation may yield interesting insights into the glass transition phenomenon.

For the PEO model, we have demonstrated that a straightforward study of the conformational relaxation is possible, when mapping the continuous trajectories of the dihedral angles onto discrete sequences of the dihedral states. Various results have indicated a complex nature of the conformational dynamics. In particular, for both dihedral species and for all dihedral states, the probability distributions of the waiting times t_w, i.e., of the time intervals between two subsequent conformational transitions, strongly deviate from an exponential function, indicating that a Markov process does not apply to the conformational dynamics. To analyze the origin of this behavior, we have discriminated between backward and forward jumps; i.e., we have distinguished whether or not the dihedrals are in the same conformational state after exactly two transitions. This analysis revealed that the nonexponential waiting-time distributions are a consequence of correlated forward–backward jumps, which are an important aspect of the conformational dynamics at sufficiently low temperatures.

Consistent with previous results for all-atom polymer models,[5] we have observed that the mean waiting times show a weaker temperature dependence than the time constants of the conformational and structural relaxations. Hence, it is not possible to explain the glassy slowdown on the basis of single events, but it is necessary to correlate the times and the directions of several consecutive conformational transitions. Analyzing the directions of subsequent transitions, we have shown that the probability of backward jumps increases upon cooling, and hence, the exploration of the conformational states is slower at lower temperatures due to both longer waiting times and higher backjump probabilities. To obtain insights into the times of consecutive transitions, we considered probability distributions $z_x(n,t)$ of finding n transitions in a time interval t. In this way, we have revealed that the conformational dynamics resembles a Poisson process at high temperatures. However, when the temperature is decreased, dynamical heterogeneities become important for the conformational relaxation and the dihedrals start having a preferred conformational state at a given time. After an exit of the preferred state state, the dihedrals show a high tendency to return to this state via a correlated backward jump. At the studied temperatures, the dihedrals remember this preferred state for up to about 30 conformational transitions. In other words, the conformational states are not sampled according to their statistical weights in the early stages of the conformational relaxation.

Acknowledgment. The author thanks the Deutsche Forschungsgemeinschaft (DFG) for funding through Grant VO 905/3-1 and A. Heuer for computer time.

References and Notes

(1) Ediger, M. D.; Angell, C. A.; Nagel, S. R. *J. Phys. Chem.* **1996**, *100*, 13200.
(2) Binder, K. *J. Non-Cryst. Solids* **2000**, *274*, 332.
(3) Glotzer, S. C. *J. Non-Cryst. Solids* **2000**, *274*, 342.
(4) Debenedetti, P. G.; Stillinger, F. H. *Nature (London)* **2001**, *410*, 259.
(5) Paul, W.; Smith, G. D. *Rep. Prog. Phys.* **2004**, *67*, 1117.
(6) Baschnagel, J.; Varnik, F. *J. Phys.: Condens. Matter* **2005**, *17*, R851.
(7) Smith, G. D.; Bedrov, D. *J. Polym. Sci., Part B: Polym. Phys.* **2007**, *45*, 627.
(8) Colmenero, J.; Narros, A.; Alvarez, F.; Arbe, A.; Moreno, A. J. *J. Phys.: Condens. Matter* **2007**, *19*, 205127.
(9) Götze, W.; Sjogren, L. *Rep. Prog. Phys.* **1992**, *55*, 241.
(10) Kob, W.; Andersen, H. C. *Phys. Rev. E* **1995**, *52*, 4134.
(11) Horbach, J.; Kob, W. *Phys. Rev. E* **2001**, *64*, 041503.
(12) Krushev, S.; Paul, W. *Phys. Rev. E* **2003**, *67*, 021806.
(13) Paul, W.; Bedrov, D.; Smith, G. D. *Phys. Rev. E* **2006**, *74*, 021501.
(14) Adam, G.; Gibbs, J. H. *J. Chem. Phys.* **1965**, *43*, 139.
(15) Garrahan, J. P.; Chandler, D. *Phys. Rev. Lett.* **2002**, *89*, 035704.
(16) Böhmer, R.; Chamberlin, R. V.; Diezemann, G.; Geil, B.; Heuer, A.; Hinze, G.; Kuebler, S. C.; Richert, R.; Schiener, B.; Sillescu, H.; Spiess, H. W.; Tracht, U.; Wilhelm, M. *J. Non-Cryst. Solids* **1998**, *235*, 1.
(17) Sillescu, H. *J. Non-Cryst. Solids* **1999**, *243*, 81.
(18) Ediger, M. D. *Annu. Rev. Phys. Chem.* **2000**, *51*, 99.
(19) Tracht, U.; Wilhelm, M.; Heuer, A.; Feng, H.; Schmidt-Rohr, K.; Spiess, H. W. *Phys. Rev. Lett.* **1998**, *81*, 2727.
(20) Reinsberg, S. A.; Qiu, X. H.; Wilhelm, M.; Spiess, H. W.; Ediger, M. D. *J. Chem. Phys.* **2001**, *114*, 7299.
(21) Qiu, X. H.; Ediger, M. D. *J. Phys. Chem. B* **2003**, *107*, 459.
(22) Kob, W.; Donati, C.; Plimpton, S. J.; Poole, P. H.; Glotzer, S. C. *Phys. Rev. Lett.* **1997**, *79*, 2827.
(23) Doliwa, B.; Heuer, A. *Phys. Rev. Lett.* **1998**, *80*, 4915.
(24) Donati, C.; Glotzer, S. C.; Poole, P. H. *Phys. Rev. Lett.* **1999**, *82*, 5064.
(25) Donati, C.; Glotzer, S. C.; Poole, P. H.; Kob, W.; Plimpton, S. J. *Phys. Rev. E* **1999**, *60*, 3107.
(26) Bennemann, C.; Donati, C.; Baschnagel, J.; Glotzer, S. C. *Nature (London)* **1999**, *399*, 246.
(27) Glotzer, S. C.; Novikov, V. N.; Schrøder, T. B. *J. Chem. Phys.* **2000**, *112*, 509.
(28) Gebremichael, Y.; Schrøder, T. B.; Starr, F. W.; Glotzer, S. C. *Phys. Rev. E* **2001**, *64*, 051503.
(29) Gebremichael, Y.; Vogel, M.; Glotzer, S. C. *J. Chem. Phys.* **2004**, *120*, 4415.
(30) Donati, C.; Douglas, J. F.; Kob, W.; Plimpton, S. J.; Poole, P. H.; Glotzer, S. C. *Phys. Rev. Lett.* **1998**, *80*, 2338.
(31) Aichele, M.; Gebremichael, Y.; Starr, F. W.; Baschnagel, J.; Glotzer, S. C. *J. Chem. Phys.* **2003**, *119*, 5290.
(32) Qian, J.; Hentschke, R.; Heuer, A. *J. Chem. Phys.* **1999**, *110*, 4514.
(33) Giovambattista, N.; Buldyrev, S. V.; Starr, F. W.; Stanley, H. E. *Phys. Rev. Lett.* **2003**, *90*, 085506.
(34) Vogel, M.; Glotzer, S. C. *Phys. Rev. Lett.* **2004**, *92*, 255901.
(35) Vogel, M.; Glotzer, S. C. *Phys. Rev. E* **2004**, *70*, 061504.
(36) Teboul, V.; Monteil, A.; Fai, L. C.; Kerrache, A.; Maabou, S. *Eur. Phys. J. B* **2004**, *40*, 49.
(37) Borodin, O.; Smith, G. D. *Macromolecules* **2000**, *33*, 2273.
(38) Borodin, O.; Smith, G. D.; Bandyopadhyaya, R.; Byutner, O. *Macromolecules* **2003**, *36*, 7873.
(39) Gray, F. M. *Solid Polymer Electrolytes*; Wiley: New York, 1991.
(40) Neyertz, S.; Brown, D. *J. Chem. Phys.* **1995**, *102*, 9725.
(41) Müller-Plathe, F.; van Gunsteren, W. F. *J. Chem. Phys.* **1995**, *103*, 4745.
(42) Catlow, C. R. A.; Mills, G. E. *Electrochim. Acta* **1995**, *40*, 2057.

(43) Lin, B.; Boinske, P. T.; Halley, J. W. *J. Chem. Phys.* **1999**, *105*, 1668.
(44) Smith, G. D.; Yoon, D. Y.; Jaffe, R. L.; Colby, R. H.; Krishnamoorti, R.; Fetters, L. J. *Macromolecules* **1996**, *29*, 3462.
(45) Ahlström, P.; Borodin, O.; Wahnström, G.; Wensink, E. J. W.; Carlsson, P.; Smith, G. D. *J. Chem. Phys.* **2000**, *112*, 10669.
(46) Borodin, O.; Douglas, R.; Smith, G. D.; Trouw, F.; Petrucci, S. *J. Phys. Chem. B* **2003**, *107*, 6813.
(47) Borodin, O.; Smith, G. D.; Douglas, R. *J. Phys. Chem. B* **2003**, *107*, 6824.
(48) Hackett, E.; Manias, E.; Giannelis, E. P. *Chem. Mater.* **2000**, *12*, 2161.
(49) Kuppa, V.; Manias, E. *J. Chem. Phys.* **2003**, *118*, 3421.
(50) Borodin, O.; Smith, G. D. *J. Phys. Chem. B* **2003**, *107*, 6801.
(51) Smith, G. D.; Borodin, O.; Bedrov, D. *J. Phys. Chem. A* **1998**, *102*, 10318.
(52) In ref 50, the correct values of the torsional parameters k_3 for the OCCH and HCCH dihedrals are −0.28 each.
(53) (a) Lindahl, E.; Hess, B.; van der Spoel, D. *J. Mol. Mod.* **2001**, *7*, 306. (b) Berendsen, H. J. C.; van der Spoel, D.; van Drunen, R. *Comput. Phys. Commun.* **1995**, *91*, 43.
(54) Hess, B.; Bekker, H.; Berendsen, H. J. C.; Fraaije, J. G. E. M. *J. Comput. Chem.* **1997**, *18*, 1463.
(55) Essman, U.; Perela, L.; Berkowitz, M. L.; Darden, T.; Lee, H.; Pedersen, L. G. *J. Chem. Phys.* **1995**, *103*, 8577.
(56) Parrinello, M.; Rahman, A. *J. Appl. Phys.* **1981**, *52*, 7182.
(57) (a) Nosé, S. *Mol. Phys.* **1984**, *52*, 255. (b) Hoover, W. G. *Phys. Rev. A* **1985**, *31*, 1695.
(58) Vogel, M.; Torbrügge, T. *J. Chem. Phys.* **2006**, *125*, 164901.
(59) (a) Vogel, H. *Z. Phys.* **1921**, *22*, 645. (b) Fulcher, G. S. *J. Am. Ceram. Soc.* **1928**, *8*, 339. (c) Tammann, G.; Hesse, W. *Z. Anorg. Allg. Chem.* **1926**, *156*, 245.
(60) Bergman, R.; Börjesson, L.; Torell, L. M.; Fontana, A. *Phys. Rev. B* **1997**, *56*, 11619.
(61) Leon, C.; Ngai, K. L.; Roland, C. M. *J. Chem. Phys.* **1999**, *110*, 11585.
(62) Sidebottom, D. L.; Johari, G. P. *J. Polym. Sci., Part B* **1991**, *29*, 1215.
(63) Gleim, T.; Kob, W. *Eur. Phys. J. B* **2000**, *13*, 83.
(64) Sidebottom, D. L.; Bergman, R.; Börjesson, L.; Torell, L. M. *Phys. Rev. Lett.* **1992**, *68*, 3587.
(65) Smith, G. D.; Yoon, D. Y.; Wade, C. G.; O'Leary, D.; Chen, A.; Jaffe, R. L. *J. Chem. Phys.* **1997**, *106*, 3798.

MA7024072